J Mater Sci: Mater Med (2006) 17:875–884
DOI 10.1007/s10856-006-0176-9

Nano-structural bioactive gradient coating fabricated by computer controlled plasma-spraying technology

C. Y. Ning · Y. J. Wang · W. W. Lu · Q. X. Qiu · R. W. M. Lam · X. F. Chen · K. Y. Chiu · J. D. Ye · G. Wu · Z. H. Wu · S. P. Chow

Received: 17 June 2005 / Accepted: 23 August 2005

Abstract The poor mechanical property of hydroxyapatite was the major problem for load bearing and implant coating in clinical applications. To overcome this weakness, a bioactive gradient coating with a special design composition of hydroxyapatite (HA), ZrO_2, Ti, bioglass was developed. This 120 μm coating with an upper layer of 30–50 μm porous HA produced by computer controlled plasma spraying which maintained energy level of the plasma which ensure proper melting of powder. The crystal size of the coating was 18.6–26.2 nm.

Transformation of t-ZrO_2 to m-ZrO_2 reduced the thermal stress that weakened the coating and lowered down interfacial strength of the coating and metal substrate. Thermal stress of sprayed coating was 16.4 MPa which was much smaller than the sample without thermal treatment of 67.1 MPa. Interfacial strength between the coating and metal substrate was 53 MPa which is much higher than conventional Hydroxyapatite coating.

Based on XRD analysis crystallinity of HA approached 98%. Therefore, high temperature treatment improved long term stability of the coating through improved crystallinity of hydroxyapatite and reduced other impure calcium phosphate phase.

C. Y. Ning
Department of Orthopaedics & Traumatology, the University of Hong Kong, Hong Kong, and Institute of Materials Science and Engineering, South China University of Technology, Guangzhou, P.R. China

Y. J. Wang · X. F. Chen · J. D. Ye · G. Wu
Institute of Materials Science and Engineering, South China University of Technology, Guangzhou, P.R. China

W. W. Lu (✉) · R. W. M. Lam · K. Y. Chiu · S. P. Chow
Department of Orthopaedics & Traumatology, the University of Hong Kong, Hong Kong
e-mail: wwlu@hkusua.hku.hk

Q. X. Qiu · Z. H. Wu
Department of Orthopaedic Surgery, Peking Union Medical College Hospital, P.R. China

1. Introduction

Hydroxyapatite (HA, $Ca_{10}(PO_4)_6(OH)_2$) is an osteoconductive and osteoinductive ceramic. It promotes strong biological bonding between implants and bone tissue [1]. However, poor mechanical properties of HA (fracture toughness of 1 $MPam^{-2}$) is the major limiting factor for load bearing application [2–5]. HA coated on a metal substrate is believed to combine the bioactivity of HA and strength of the metal [6]. Osteoconductive and bioactive HA coating provides a reliable interface between bone tissue and implant [7–9]. In addition, significant metallic ions release reduction under the physiological environment. Various deposition techniques have been attempted to achieve an optimal bioactive coating properties including plasma spraying [10, 11], electrocrystallization [12], pulsed laser deposition [13, 14], ion beam deposition [15], magnetron sputtering [16], sol-gel [17] and biomimetic techniques [18]. Among them, the plasma-spraying technique has been the most popular since it is efficient and economical. However, the poor bond strength between the HA coating and the metal substrate introduce potential weakness point in the prosthesis system [19]. The bond strength is mainly affected by the physical and chemical properties difference between the coating and the metal substrate. Thermal coefficient difference between the metal and HA combined with the rapid cooling down of spray droplets lead to residual stress in the coating. Surface chemical composition and topography also affect the coating stability and

bonding strength with the bone tissue in a physiological environment [20–22]. The surface roughness of the HA coating plays a vital role in its physicochemical reaction with bone. Different morphological dimensions are important and affect the process of endosseous integration in various ways, including the activation, adhesion, orientation, morphology, and movement of the cells. Wennerberg [23, 24] reported that using an implant with roughness between 0.5 and 1.5 μm resulted in an ideal balance between surface enlargement and ion leakage.

Various composite coatings on metal have been studied to improve the bonding strength of a coating under physiological condition, Ding studied a series of HA/BG composite coatings on titanium alloy substrate. Lei used yttria-stabilized zirconia to reinforce hydroxyapatite coatings. Compared with regular HA coating, the bioactive gradient coating with continuous gradient metal–ceramic composites can improve interfacial bonding between dissimilar solids, minimize thermal stresses, reduce the effective driving force for fracture, arrest cracks, and increase the long-term stability in the physiological environment. In this study, we aimed to develop the bioactive gradient coating (BGC) contain nano HA, ZrO_2, and Al_2O_3, to deposit on a titanium substrate using the net-energy plasma-spray technique and to evaluate the surface characterizations. The morphology and phases of the surface in BGC were investigated using AFM, SEM and XRD. The profile of the BGC topography was identified with a surface profile apparatus. The hypothesis in the present study was BGC coating combine with thermal treatment will improve the mechanical strength via reduction of thermal stress, increasing coating fracture toughness and bonding strength.

2. Materials and methods

Nano-crystalline HA powder was prepared by adding 0.2 M $Ca(NO_3)_2$ into 0.1 M $(NH_4)_2HPO_4$ solution. The resultant HA precipitate underwent aging, centrifugation, and drying. It was heated at 850°C for 0.5 h to obtain nano-crystal integrated hydroxyapatite. Spherical shape nano-crystalline ZrO_2 powder was synthesized by hydrothermal process at 90°C by adding 2 M NaOH solution into $ZrOCl_2 \cdot 8H_2O$ solution. Ti and Al_2O_3 were obtained commercially (Miller Thermal, USA) with average particles sizes of 30 and 34 μm respectively. Prior to plasma spray, the commercially available Ti-6Al-4V substrate was sandblasted with 400 μm Al_2O_3 particles and then ultrasonically cleaned in analytic reagent acetone solution.

The bioactive gradient coatings (BGC) were deposited by a robotically controlled plasma-spraying machine (Praxair 4500, Praxair Surface Technologies, USA) equipped with an advanced computerized closed-loop powder feed system.

Table 1 Plasma spraying parameters for depositing bioactive gradient coating

Spraying parameters	Value of parameters
Primary gas	Argon 90 scfh
Auxiliary gas	Hydrogen 12 scfh
Carrier gas	Argon 25 scfh
Spraying currents	650 A
Spraying volts	35 V
Standoff distance	100 mm

The main plasma spraying parameters used in this study were listed in Table 1.

BGC was fabricated by altering the ratio of HA, Ti, Al_2O_3 and ZrO_2 with a computer-controlled powder feed system. The coating had a thickness in the range of 120 μm with the gradient coating contained HA, Ti, Al_2O_3 and ZrO_2.

Phases of the BGC surface were analyzed by an X-ray diffractometer (XRD, D8GADDS, Brucker Corp) with CuKα radiation at 40 kV and 30 mA, scanning in the standard θ to 2θ geometry from 10° to 80° at step size of $0.01^\circ\,s^{-1}$. The crystalline sizes of the initial HA powder and BGC were obtained from broadening of the (002 diffraction line that related to c-axis of hydroxyapatite) diffraction peak using the Scherrer equation. The topography and microchemistry of the coating were performed with a SEM (Cambridge Stereo Scan 360) equipped with an energy dispersive spectroscopy (EDS, OXFORD detector) system. The topography of the surface of the coating was observed using Atom Force Microscopy (Nanoscope II, Digital Instruments). The roughness of the coating's surface was measured using a surface profile apparatus (KLA-TENCOR Alpha-Step 500, TRITEK Corp, USA).

$$t_{(hkl)} = \frac{0.94\lambda}{\cos\theta_{hkl}\sqrt{D^2 - D_0^2}} \quad (1)$$

The crystal size of HA powder and coating were measured by XRD peak broadening and calculated based on the Scherrer equation: where $t_{(hkl)}$ is the crystal size (nm); λ is the wavelength of the monochromatic X-ray beam (nm, $\lambda_{k\alpha Cu} = 0.15418$ nm); D is the full length at half maximum for peak sample under consideration [rad]; D_0 is the full length at half maximum for peak standard under consideration [rad]; and $\theta_{(hkl)}$ is the exact diffraction satisfying the Bragg's law for the (hkl) Miller's plane [°]. The peak corresponding to the (002) Miller's plane is sharper than other peaks in the XRD pattern. According to equation (1) the mean sizes of the HA crystal were calculated. According to XRD analysis, plasma spraying process reduced the crystalline size.

Mechanical properties of the coating were analyzed by XRD and MTS 810 (according to ASTM C 633-79 standard) XRD was used to analyze the residual stress by following parameter. The face of crystal analyzed is 526 on

the hydroxyapatite and $2\Theta = 141.325^\circ$ and operating voltage and current was 40 kV and 100 mA respectively. Ψ angle is picked at 0, 15, 30 and 45.

Interfacial bonding strength was analyzed with MTS 810. Each group contained 6 specimens and averaging was taken to reduce fluctuation between different specimens. The detail of interfacial bonding testing was shown in Fig. 6.

Thermal stress was analyzed by XRD analysis from hkl peak shifting analysis from six samples average value was taken as test results of the residual stress of the gradient coatings.

In vivo and in vitro analysis was taken on this bioactive gradient coating. Table 2 showed that the average Ca:P ratio of the coating 1.72 and some special feature flat was 1.86. Since the value was higher than 1.67 normal hydroxyapatite Ca:P ratio due to two main reasons, some unavoidable decomposition in spraying process and addition of other ZrO_2 form other compounds. Immersion in stimulate biological fluid was taken for 500 h period and weight loss was measured. For animal study 9 dogs were used with weigh of 12–15 kg. 60 Ti6Al4V rods were used in this animal 40 of them was coated with bioactive gradient coating half of them were further treated with rhBMP-2. First group was inserted with Ti6Al4V as control, second group was inserted with Ti6Al4V with bioactive gradient coating and third group was inserted with rhBMP-2 with bioactive gradient coating. The incision site is on the hip region the whole operation the animal was disinfected with iodine solution and sedated with barbiturate salt 30 mg/Kg injection. The metal rod was implanted in femur of the dog by drilling a hole with saline washing. To avoid infection after operation, penicillin was given through intra muscular injection. One animal in each group was sacrifice after 3, 6 and 16 week after operation for histomorphology analysis.

For implant-bone interface we analyze the shearing strength based on push out test. The test was carried out by SWD-10 machinery. The sample bone membrane was removed exposed the implant surface. The sample was clamped on the v-shaped holder the rate to push out with specialize needle at a rate of 1 mm/min to pull out the implant.

The shearing strength = Maximum force divided by bone-implant interface area.

3. Results

3.1. Phase purity

The schematic drawing of the bioactive gradient coating and the microstructure were shown in Fig. 1. The XRD pattern (Fig. 2) indicates that traces of $Ca_2P_2O_7$ and CaO phase were detected on the BGC surface. Comparing the XRD pattern of BGC with that of initial HA powders for spraying (Fig. 2a and b), apparently large amounts of amorphous phase was formed during the plasma spraying process.

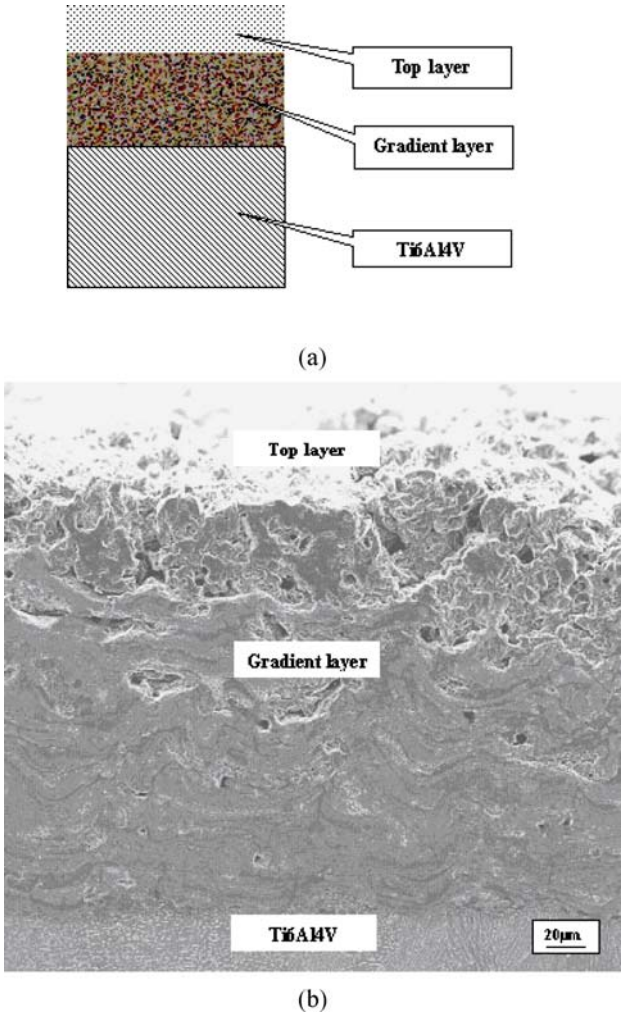

Fig. 1 Schematic drawing of (a) cross-sectional view (b) SEM of bioactive gradient coating with continuous variety in microstructure and compositions.

3.2. Micromorphology observation

Figure 3 presents the surface roughness profile of BGC. The surface of the BGC was considered very rough (+10 to $-20\ \mu$m). Figure 4 shows the surface microstructure characteristic of AS-SPRAYED BGC. The Ca/P ratios of different point/area in the BGC were analyzed using SEM-EDS equipment (Table 2). SEM photographs revealed that the BGC

Table 2 Ratio of Ca/P of different point/area in the surface of AS-SPRAYED BGC

Area for EDS	Ratio of Ca/P
Whole coating	1.72
Area of flat	1.86
Particle A	1.67
Particle B	1.67

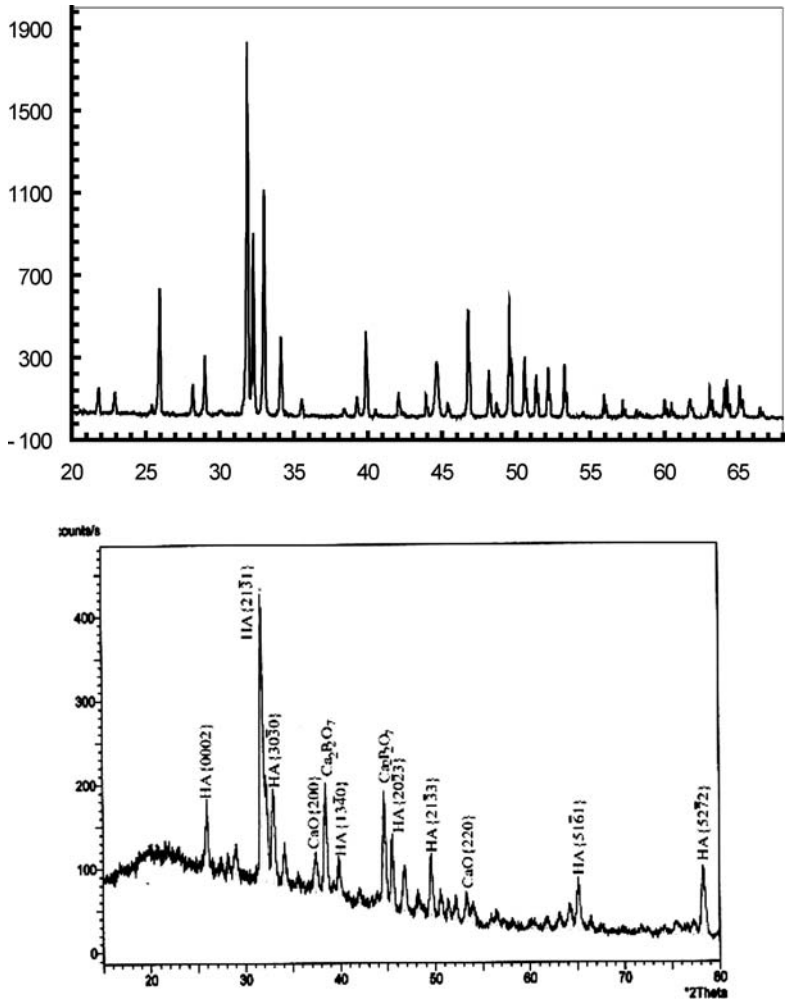

Fig. 2 XRD pattern of (a) HA powders (b) AS-SPRAYED coating.

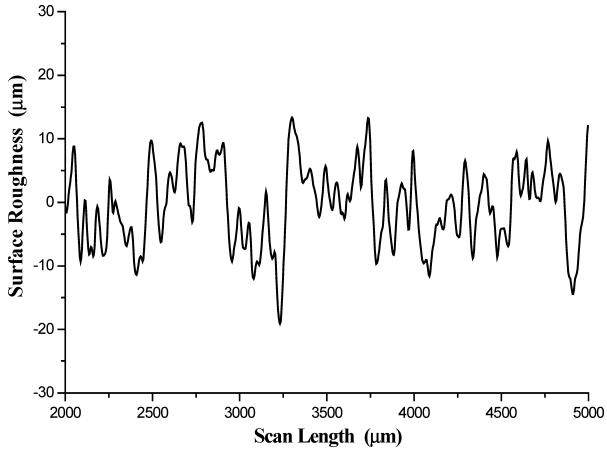

Fig. 3 Surface roughness profile of bioactive gradient coating.

possessed typical features of plasma-sprayed coating. Flats, pores, particles, and caves with different size and shape were observed. Many nanometer-sized grains were observed on the surface of the flats in SEM photographs, in which the Ca/P ratio of the particles was 1.67, demonstrating the presence of HA particles.

3.3. Chemical composition variation

The Ca/P ratio of the flat was 1.86, which indicates that P_2O_5 may be lost from the powder during spraying with higher torch power. The flats with less porosity were tightly bonded with the coating. Some solid and partially-melted particles were embedded into the melted splats, appearing as spheres.

AFM was used to characterize the topography of the bioactive gradient coating (Fig. 5). The AFM images show that flat surface was rough and consisted of many irregular nanometer-sized grains. The rough nanometer-sized structure could provide higher specific surface area and bonding capacity for cell adhering and culturing.

Based on the above equation (1), the mean sizes of the HA crystal were calculated and listed in Table 3. After plasma spraying, the crystal sizes became smaller. The metastable amorphous phase presented as sprayed BGC tended to recrystallize.

The upper layer of the coating is purely rough and porous hydroxyapatite with thickness of 30–50 μm. The intermediate layer was a mixture of hydroxyapatite, bioglass (Al_2O_3,

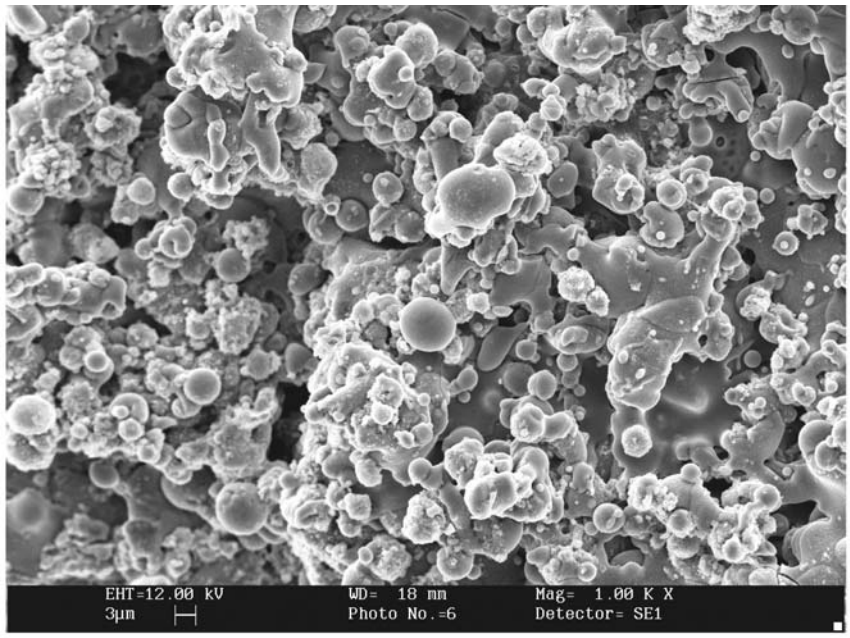

a

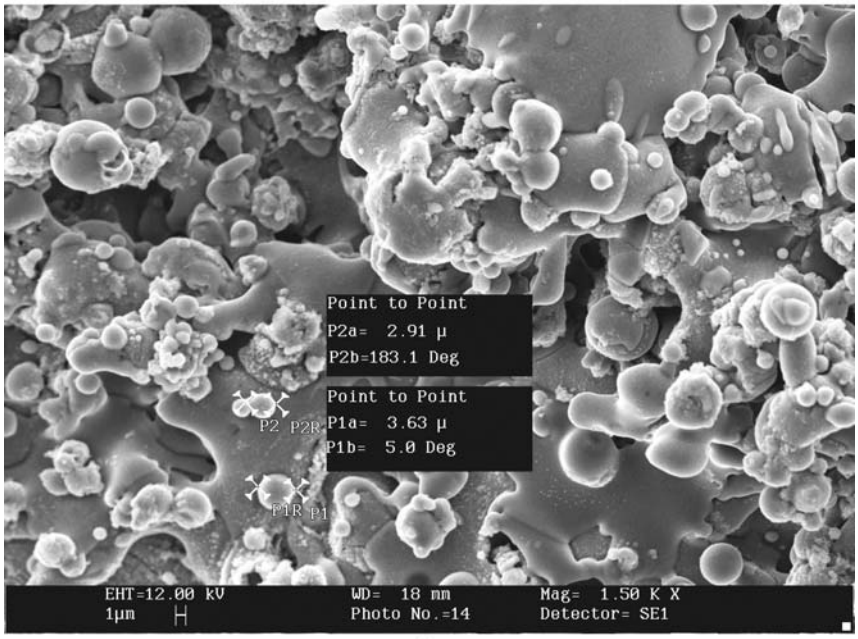

b

Fig. 4 SEM micrographs of the AS-SPRAYED bioactive gradient coatings. (a) Overview of the coating's surface with low magnification (Mag = 1000); (b) Overview of the coating's surface with high magnification (Mag = 1500); (c) Un-melted powder embedded into the melted splat (Mag = 10000); (d) Un-melted spherical powder attached on the surface of melted splat (Mag = 13400); (e) Melted flat with nano-size microstructure (Mag = 3290); (f) Nano-size grain on melt flat (Mag = 13170).

Table 3 Crystal size of the HA powder and the surface of AS-SPRAYED BGC

Samples	Crystal size (nm)
Initial HA powders	25.0 ∼ 40.0
Surface of BGC	18.6 ∼ 26.2

P_2O_5) and ZrO_2. The gradient change of the coating is uniform and can be verified from the EDX result. Near the metal substrate, the Young's modulus rise and was finally close to Ti value.

Interfacial strength was shown on Table 4. It was shown that with heat treatment the gradient bioactive hydroxyapatite coating had highest interfacial strength compare with other groups. Heat treatment reduced CaO and other impure phase concentration and convert them to crystalline hydroxyapatite. This process produced nano crystalline hydroxyapatite which is stronger than amorphous phase.

Residual stress of the gradient coating was shown on Table 5. It was shown that gradient coating has lower thermal stress due to lower different in thermal expansion coefficient and elastic modulus. The different in thermal

Fig. 4 *(Continued).*

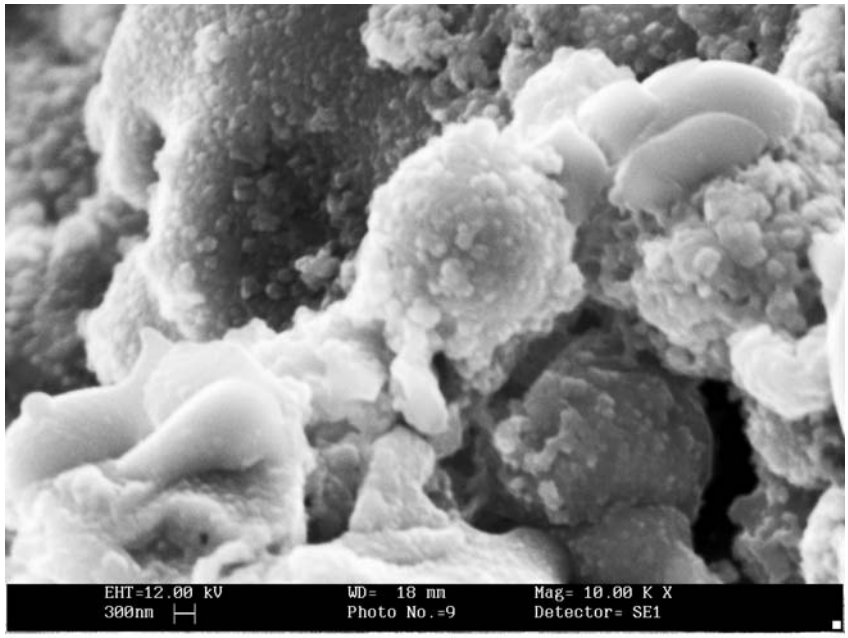

c

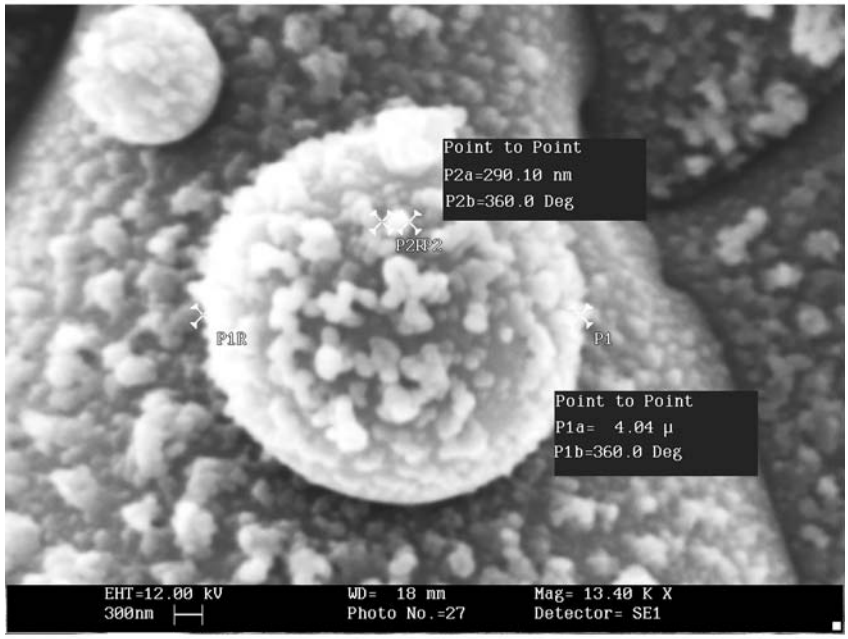

d

Table 4 Interfacial bond strength of the coatings (ASTM C633-79)

Sample	Strength (MPa)
Gradient Hydroxyapatite coating spraying	40
Gradient Hydroxyapatite coating with heat treatment	53
Hydroxyapatite plasma coating	19
Hydroxyapatite plasma coating with heat treatment	22

coefficient lead to stress build up in the cooling of coating when plasma melted particle hit the cold metal substrate. Heat treatment eliminated some of the thermal stress by conversion of new phase $CaTiO_3$ and $CaZrO_3$ and slow cooling process in heat treatment allow crystal structure reorganization.

For animal study the dog did not show any wound infection. Feeding of the dogs was good. Dogs had shown

Fig. 4 *(Continued).*

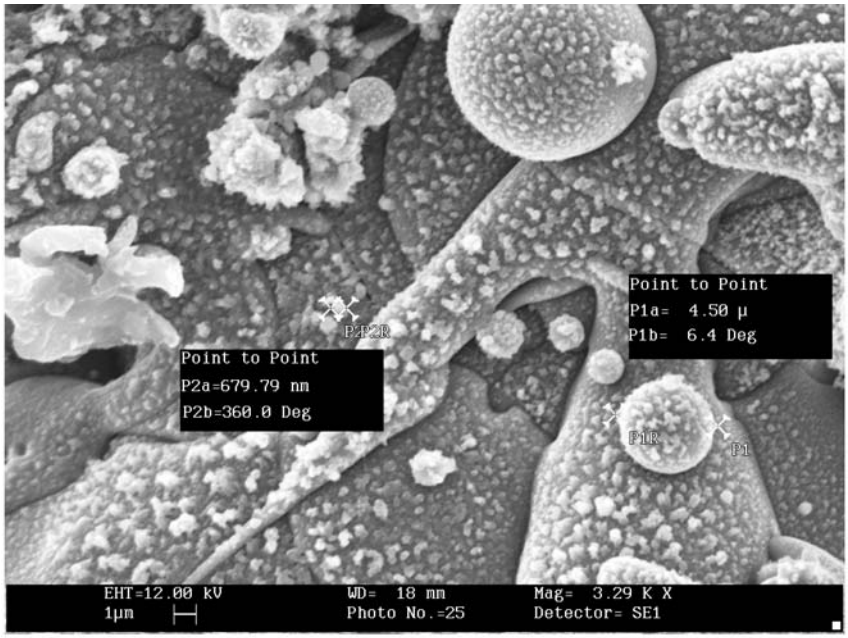

e

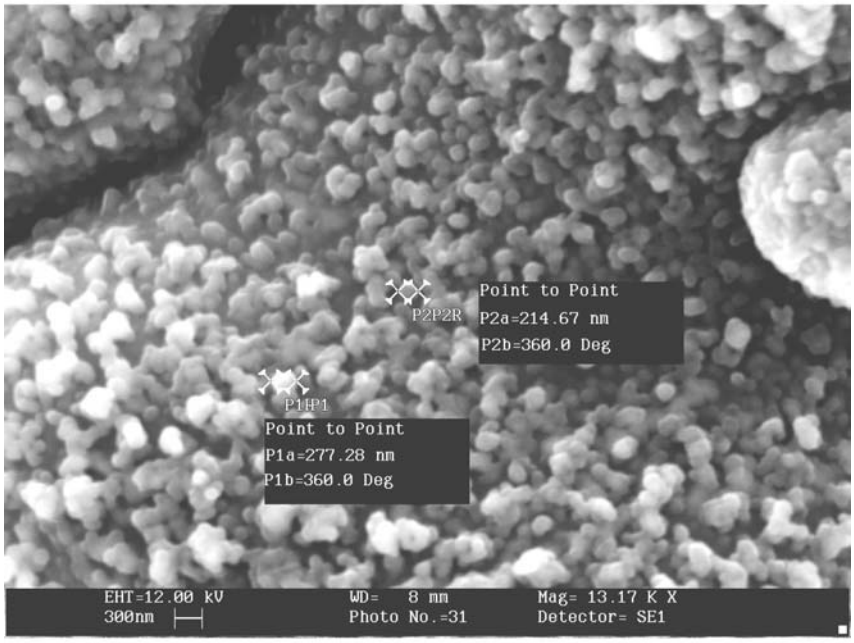

f

Table 5 Test results of the residual stress of the gradient coatings

Sample	Residual stress of gradient coating (MPa)
Hydroxyapatite gradient coating	67.054
Hydroxyapatite coating	394.348
Hydroxyapatite gradient coating with heat treatment	16.361
Hydroxyapatite coating with heat treatment	305.275

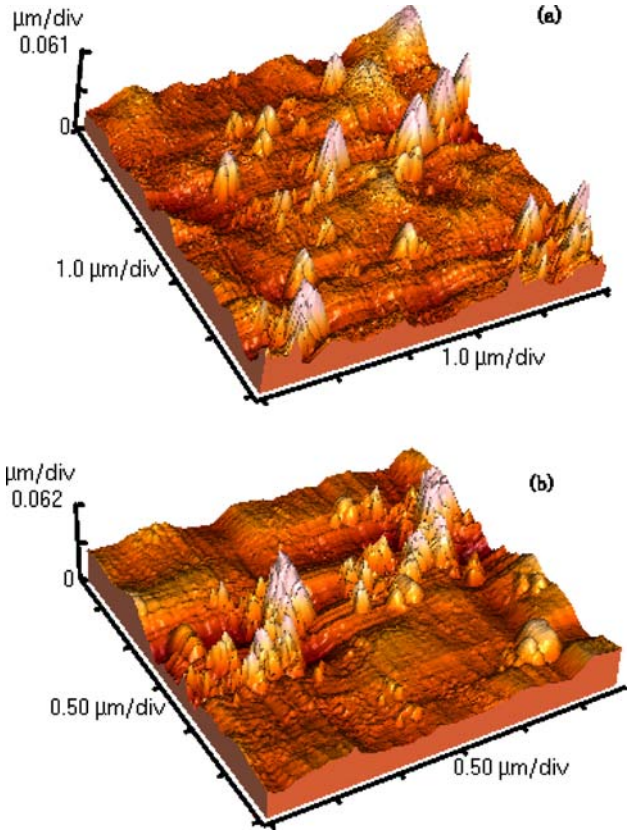

Fig. 5 3D AFM topography of bioactive gradient coating shows the nano-size surface structure. (a) 3D nano-size structure in the surface of a particle (refer to Fig. 4d); (b) 3D nano-size structure in the melted flat area (refer to Fig. 4f).

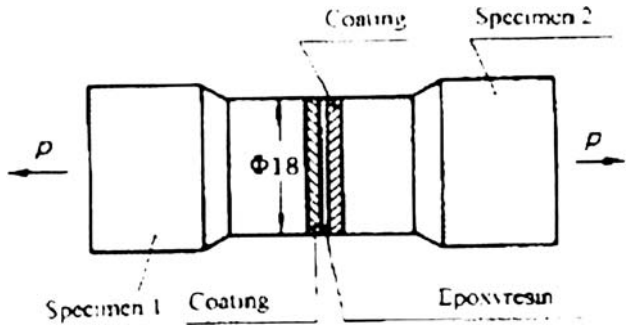

Fig. 6 ASTM testing set drawing.

different degree of weight gain. The implant had no loosening and based on radiological analysis there were no sign of bone resorption near the implant. From histological analysis based on PMMA embedded implant section there were no fiber tissue invasion and oseteoblast and new blood vessel was observed in the section.

The weight loss based on 500 hrs immersion in stimulate biological fluid only shown 0.2% weight loss it reflected that coating was stable within biological system.

The bone-coating interfacial strength was shown in Fig. 7 it shown that bioactive gradient coating with rhBMP-2 shown higher interfacial bonding strength at 6 week after that rhBMP-2 effect fade out. With coating the interfacial bonding strength between bone and coating was much higher than pure Ti6Al4V.

4. Discussion

Thermal stress is the major failure cause of HA coating. It is caused by CTE difference (coefficient of thermal expansion) between HA and metal substrate. Some modification of coating composition was taken to resolve this problem such as adding mechanical strength enhancer yttria stabilized zironia [25]. ZrO_2 set up compressive stress fields around itself, which aided crack deflection and improved the interfacial strength between the secondary particles and matrix. CaO diffusion enhances the t-ZrO_2 conversion to c-ZrO_2. In the spraying process, formation of $CaZrO_3$ was the major change in coating structure and bonding method.

The phase compositions of plasma-sprayed HA coatings have been well documented [26–28]. The major constituent of the coating was hydroxyapatite with traces of decomposed pyrophosphate phase. There was a significant difference in the results of phase composition, which could be ascribed to the use of different plasma-sprayed parameters. Generally higher plasma net energy leads to higher amorphous phase formation and decomposition of hydroxyapatite to oxyapatite [29] and tri-calcium phosphate. The plasma spraying process involves complex thermal exchanges between the plasma zone, powder particles, and substrate. Particles injected into the 10,000°C plasma jet underwent an extremely high heating rate within a few microseconds. Although the powder did not reach the plasma flame temperature, the particles may melt or even boil at their surface layer. In terms of the equilibrium phase diagram for the system Ca-P_2O_5-H_2O, the degradation of HA was unavoidable.

BGC coating after net energy spraying process has two phases before heat treatment. From the FTIR diagram, some hydroxyl group was removed in the high temperature spraying process. Most amorphous phase can be converted to nano crystalline phase with a suitable period of high temperature treatment. Formation of crystalline HA phase is beneficial to coating bioactivity by reducing more soluble amorphous phase. This reduces coating susceptibility to dissolution.

During the plasma spraying, the samples remained at a relatively high temperature for some time after the spraying process ended. Therefore, it is reasonable to surmise that the fine nano-sized grains with Ca/P ratio of 1.67 on the surface of the splat, as shown in the SEM photographs, were formed from the metastable amorphous phase. Dong ZL *et al.*

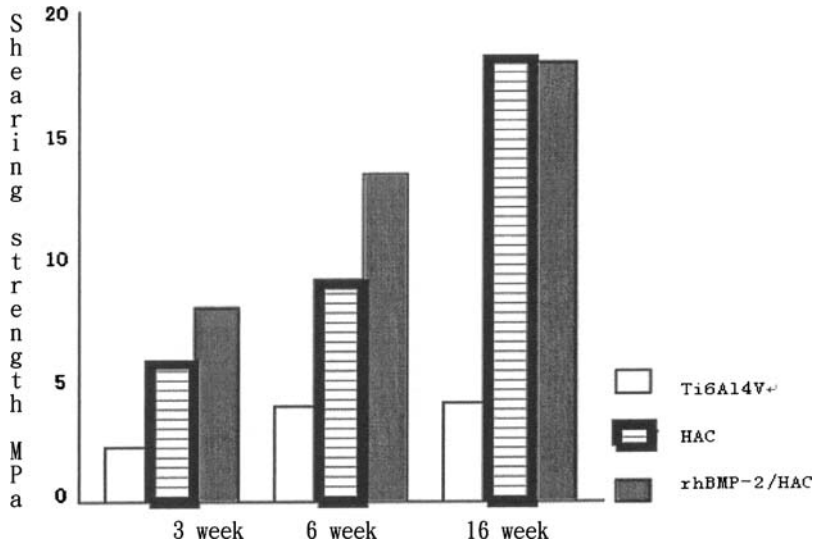

Fig. 7 Shearing strength of coating and bone interface.

[30] used TEM techniques to verify that HA nano-particles were grown from the amorphous phase area, which was in agreement with our results.

5. Conclusions

In this study bioglass, ZrO_2 and HA composite gradient coating with high temperature treatment show great improvement in long term stability via reduction in thermal stress and coating solubility. Interfacial strength between coating and metal substrate was significantly improved from 19 to 53 MPa. ZrO_2 reduces thermal stress by shifting to a different phase to compensate for the difference in thermal expansion coefficient while the bioglass intermediate layer provides a choice of a variable range of thermal coefficient thorough composition adjustment. The surface of the coating showed typical features of plasma-sprayed coating with nano-crystalline grains. High temperature treatment coating has improved mechanical performance compared with untreated sample with thermal stress level drops from 67.1 to 16.4 MPa.

Acknowledgments The authors would like to acknowledge the financial support of National Natural Science of China (No. 59932050 and 59872010), and HKRGC (HKU7290/00M).

References

1. R. R. LORENZ, F. A. PAPAY, M. JATLA, S. W. BARTHEL and B. M. SEELEY, *J. Craniofac. Surg.* **13**(6) (2002) 802.
2. M. UESHIMA, S. NAKAMURA AND K. YAMASHITA, Huge, *Adv. Mater.* **14**(8) (2002) 591.
3. W. N. CAPELLO, J. A. D'ANTONIO, J. R. FEINBERG and M. T. MANLEY, *Clin. Orthop.* **405** (2002) 92.
4. T. R. BLATTERT, G. DELLING, P. S. DALAL, C. A. TOTH, H. BALLING and A. WECKBACH, *Spine* **27**(23) (2002) 2697.
5. C. CHU, J. ZHU, Z. YIN and P. LIN, *Mater. Sci. Eng. A-Struct. Mater. Prop. Microstruct. Process.* **316** (2001) 205–210.
6. L. L. HENCH, *Bioceramics Am. Ceram. Soc.* **81**(7) (1998) 1705.
7. T. JINNO, D. T. DAVY and V. M. GOLDBERG, *J. Arthroplast* **17**(7) (2002) 902.
8. J. L. ONG, K. BESSHO and D. L. CARNES, *Int. J. Oral Maxillofac. Implants* **17**(4) (2002) 581.
9. S. C. BAYLISS, R. HEALD, D. I. FLETCHER and L. D. BUCKBERRY, *Advanced Materials* **11**(4) (1999) 318.
10. Y. P. LEE, C. K. WANG, T. H. HUANG, C. C. CHEN, C. T. KAO and S. J. DING, *Surface and Coatings Technology* **197**(2–3) (2005) 367.
11. X. NIE, A. LEYLAND, A. MATTHEWS, J. C. JIANG and E. I. MELETIS, *J. Biomed. Mater. Res.* **57**(4) (2001) 612.
12. M. SHIRKHANZADEH, M. AZADEGAN, V. STACK and S. SCHREYER, *Materials Letters* **18**(4) (1994) 211.
13. I. N. MIHAILESCU, P. TORRICELLI, A. BIGI, I. MAYER, M. ILIESCU, J. WERCKMANN, G. SOCOL, F. MIROIU, F. CUISINIER, R. ELKAIM and G. HILDEBRAND, *Applied Surface Science* **248**(1–4) (2005) 344.
14. J. M. FERNANDEZ-PRADAS, L. CLERIES, E. MARTINEZ, G. SARDIN, J. ESTEVE and J. L. MORENZA, *Biomaterials* **22**(15) (2001) 2171.
15. M. YOSHINARI, Y. OHTSUKA and T. DERAND, *Biomaterials* **15**(7) (1994) 529.
16. DING SHINN-JYH, *Biomaterials* **24**(23) (2003) 4233.
17. B. BEN-NISSAN, A. MILEV and R. VAGO, *Biomaterials* **25**(20) (2004) 4971.
18. M. STIGTER, K. DE GROOT and P. LAYROLLE, *Biomaterials* **23**(20) (2002) 4143.
19. M. WEI, A. J. RUYS, B. K. MILTHORPE, C. C. SORRELL and J. H. EVANS, *J. Sol-Gel Sci. Techn.* **21**(1–2) (2001) 39.
20. L. GLADIUS, *Bio-medical Materials and Engineering* **10**(3–4) (2000) 157.
21. D. E. MACDONALD, F. BETTS, M. STRANICK, S. DOTY and A. L. BOSKEY, *J. Biomed. Mater. Res.* **54**(4) (2001) 480.
22. S. RADIN, P. DUCHEYNE, P. BERTHOLD and S. DECKER, *J. Biomed. Mater. Res.* **39**(2) (1998) 234.

23. A. WENNERBERG, T. ALBREKTSSON and J. LAUSMAA, *J. Biomed. Mater. Res.* **30** (1996) 251.
24. A. WENNERBERG, T. ALBREKTSSON, C. JOHANSSON and B. ANDERSSON, *Biomaterials* **17** (1996) 15.
25. A.K. GAIN, H.Y. SONG and B.T. LEE, *Scripta Materialia* **54**(12) (2006) 2081.
26. B. COFFINO, P. FOGARASSY, P. MILLET and A. LODINI, *J. Biomed. Mater. Res. Part A* **70**(1) (2004) 20.
27. Y. W. GU, K. A. KHOR, D. PAN and P. CHEANG, *Biomaterials* **25**(16) (2004) 3177.
28. J. F. LI, H. L. LIAO, C. X. DING and C. CODDET, *J. Mater. Process Tech.* **160**(1) (2005) 34.
29. T. M. LEE, C. Y. YANG, E. CHANG and R. S. TSAI, *J. Biomed. Mater. Res. Part A* **71A**(4) (2004) 652.
30. C.-J. LIAO, F.-H. LIN, K.-S. CHEN and J.-S. SUN, *Biomaterials* **20**(19) (1999) 1807.